

On the material genome of wurtzite ferroelectrics

Zijian Zhou,^{1,#} Jinhai Huang,^{1,#} Kan-Hao Xue,^{1,2,*} Heng Yu,¹ Shengxin Yang,¹ Shujuan Liu,²
Yiqun Wang,² Xiangshui Miao^{1,2}

¹School of Integrated Circuits, Huazhong University of Science and Technology, Wuhan 430074, China.

²Hubei Yangtze Laboratory, Wuhan 430205, China

#These authors contributed equally.

*Corresponding author: xkh@hust.edu.cn

Abstract

As the dielectric film thickness shrinks to ~ 10 nm, some traditional wurtzite piezoelectric materials demonstrate ferroelectricity through element doping. Among them, Sc doped AlN and Mg doped ZnO are the most famous examples. While it is widely acknowledged that the dopant atoms effectively reduce the coercive field, enabling ferroelectric polarization switching, the material genome of these wurtzite (WZ) ferroelectrics is still less understood. In this work, we analyze the features of WZ ferroelectrics, ascribing them to five-coordination (5C) ferroelectrics, which may be compared with 6C ferroelectrics (perovskite-type) and 7C ferroelectrics (hafnia-like). In particular, the exact reason for their adopting the hexagonal WZ structure instead of the zinc blende structure is studied. Emphasis is paid to the degree of ionicity in promoting the hexagonal arrangement, and the phenomenon of layer distance compression is discovered and explained in WZ ferroelectrics. The role of element doping in coercive field reduction is understood within this context.

Ferroelectric non-volatile memory (FeRAM) and ferroelectric field effect transistor have emerged as effective solutions in addressing the current demand on data storage, for a balanced speed and power consumption, as well as its electric voltage-driven nature. The first commercial FeRAM products in the 1990s utilized perovskite ferroelectrics, such as $\text{PbZr}_{1-x}\text{Ti}_x\text{O}_3$ (PZT), for their sufficient spontaneous polarization and low switching barrier. Nevertheless, perovskite-type FeRAM has long been staying at the 130 nm technical node,¹ for two major reasons. On the one hand, these ferroelectrics require a relatively high crystallization temperature above 600°C, which is inconsistent with the advanced CMOS technology that usually involves metallization materials such as NiSi_x , which can only withstand 450°C to 500°C. On the other hand, the vertical scaling performance of typical perovskite ferroelectrics is unsatisfactory, which does not maintain well ferroelectricity at a thickness below 10 nm. The discovery of ferroelectricity in doped hafnia² and doped AlN,³ however, has revived the hope for high-density ferroelectric memory devices. These simple compounds can retain excellent spontaneous polarization characteristics even at scales as small as a few nanometers. Nowadays, hafnia-based ferroelectrics are classified as fluorite-type ferroelectrics, while AlN-based ferroelectrics are named wurtzite (WZ) ferroelectrics. Compared with their great application potential, the physical understanding into their origin of ferroelectricity is less mature. Recently, a theory based on chemical coordination numbers has been proposed for the emergence of ferroelectrics in fluorite-type materials, which states that the small cation radius forbids these compounds to place 8 O anions around each cation, reducing the cation coordination number from 8 to 7.⁴ An asymmetric way of forming the 7-coordination (7C, and the same short note will be used throughout) configuration leads to the ferroelectric phase. In contrast, WZ ferroelectrics own an even shorter history,⁵ and investigation into its ferroelectric material genome has been relatively rare.

Traditional WZ materials are known for their piezoelectric properties, but their ferroelectric performance has been limited by excessively high coercive fields (E_c),

which typically lead to dielectric breakdown before polarization switching can occur. The problem is alleviated with the advent of $\text{Al}_{1-x}\text{Sc}_x\text{N}$ with lower E_c values,³ sparking renewed interest in the ferroelectric properties of WZ structures. Around the same time, doping strategies in other WZ materials have been proposed to induce ferroelectricity, such as Mg-doped ZnO ^{6,7} and Sc-doped GaN .^{8,9} Among AlN-based compounds, replacing Al atoms with elements like Sc, Y¹⁰ or B^{11,12} has proven effective in lowering the switching barrier. Most explanations attribute these effects to factors like stress or volume changes, though they often remain *post hoc* interpretations. Currently, clear theoretical guidance to predict switching barrier behavior faithfully is yet to be established.

From a geometric point of view, the WZ structure consists of cations and anions arranged in a hexagonal close-packed (*h.c.p.*) configuration, leaving a finite polarization along the *c*-axis. The zinc-blende (ZB) structure, similarly, is a close relative of WZ that has a cubic close-packed (*f.c.c.*) arrangement, and ZB materials do not exhibit ferroelectricity. Meanwhile, some researchers have tried to alter the *c/a* length ratio to tune the switching behavior.^{13,14} Interestingly, different metals with *h.c.p.* structures often exhibit varying degrees of distortion,^{15,16} suggesting a potential link between WZ ferroelectricity and metal packing. The reason for the preference of a hexagonal structure against a cubic structure deserves in-depth investigation for both metals and compounds. The mechanism for a WZ ferroelectric to abandon the cubic ZB structure is accordingly key to its ferroelectric material genome. Hence, this study explores the origin of ferroelectricity in WZ structures, focusing on the selection between hexagonal WZ and cubic ZB structures by nature. And the paper is organized as follows. After introducing the basic settings involved in our calculations, the cation coordination number and lattice constant ratio of the WZ-structure binary compounds are investigated, for a relatively large set of materials. The tendency of their adopting the WZ or the ZB structure will be analyzed. Finally, the effect of doping in coercive field reduction is discussed.

Computational Details

All first-principles calculations in this study were performed using density functional theory (DFT) under generalized gradient approximation (GGA), as implemented in the Vienna *Ab initio* Simulation Package^{17,18} (VASP). The Perdew-Burke-Ernzerhof (PBE) functional¹⁹ was used to account for exchange-correlation interactions. The projector augmented-wave (PAW) method^{20,21} was applied, and the valence electrons configurations were: $2s2p$ for B/N/O, $3s3p$ for Al/P/S, $4s3d$ for Zn, $4s4p3d$ for Ga, $4s4p$ for As/Se, $5s4d$ for Cd, $5s5p4d$ for In, $5s5p$ for Sb/Te, and $6s5d$ for Hg. The WZ and ZB phases were modeled using the $P6_3mc$ and $F\bar{4}3m$ space groups, respectively. A plane-wave cutoff energy of 500 eV was set for all calculations. The k -point mesh for relaxation was $11 \times 11 \times 11$ centered at Γ . The convergence criteria for ionic relaxation was set at 0.001 eV/\AA , and the electronic energy convergence threshold was 10^{-8} eV . The climbing image nudged elastic band (CI-NEB) method was employed to compute polarization switching barriers, with force convergence set to 0.01 eV/\AA and electronic convergence at 10^{-7} eV . Additionally, the shell DFT-1/2 method²²⁻²⁴ was used to correct self-interaction errors, with inner and outer self-energy potential cutoff radii set at 0.8 and 2.4 bohr, respectively.

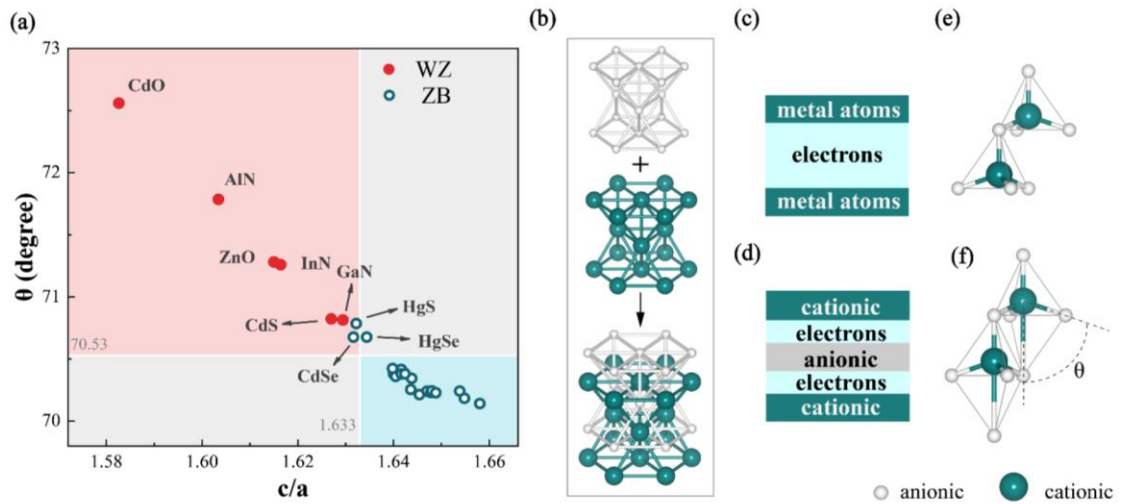


Figure 1. (a) The relationship between the structural state and its distortion. The entire diagram is divided into four regions by two reference lines: the N_5 (*cf.* the Appendix) bond angle of a regular

tetrahedron (70.53°) and the ideal c/a ratio ($\sqrt{8/3} = 1.633$) for a regular tetrahedron. The red region indicates c -axis compression, while the blue region indicates c -axis elongation. The closer a point is to the top-left corner, the stronger the compression effect in the system. (b) WZ structure. Polar plate model of the *h.c.p.* structure (c) and WZ structure (d). The polyhedron formed by nearest neighbor atoms in traditional coordination theory (e) and mixed length-angle coordination theory (f).

Results and discussion

Traditional coordination theory identifies the WZ structure as a 4C system, where cations are located within a tetrahedral arrangement of surrounding anions, similar to the ZB phase. Accordingly, it is difficult to understand the difference between WZ and ZB structures from the cation coordination number perspective. The reason lies in that the coordination number has been calculated with the sole reference to the bond lengths. Based on a tetrahedron, there is hardly any large mismatch between positive and negative charge centers, unless the ions are permitted to shuttle between neighboring tetrahedra. In that case, however, it becomes better to adopt a broader geometric picture. Recently, we have proposed a coordination number theory that refers to both the bond lengths and bond angles,⁴ and it is shown to be particularly suitable for ferroelectrics. The basic idea is (see Appendix for details), based on a central cation, to assign each neighboring anion a finite solid angle. Once the entire space is parceled out, additional anions located farther apart will no longer be counted as neighbors. Quantitatively, a new anion could be included in the neighbors only if its angle to any existing neighboring bond is greater than 65° (the reason for this threshold angle was specified in the original publication⁴). This coordination theory may be applied to analyze WZ and ZB compounds. To this end, we first arranged all IIB-VI and IIIA-V compounds to be in the (possibly hypothetical) WZ structure. After performing full structural relaxation within the hexagonal framework, the geometric data are given in **Figure 1(a)**. Among them (see data listed in **Table 1**), the one that is closest to 4C is BP. Manually set in the WZ structure, BP has the smallest fifth anion bond angle, $\theta = 70.14^\circ$, but it is

still larger than the critical 65° angle, meaning that the fifth P anion is still classified as a coordinated anion. This does not mean BP should adopt the 5C WZ structure in reality; it is naturally in the ZB structure unless constrained in the WZ configuration as in our research. To sum up, the WZ structure could be considered a 5C system²⁵ according to the mixed length-angle definition of cation coordination number. In this configuration, the anion center establishes the base of a trigonal bipyramid, while the cation is located at the center of the upper tetrahedron. The displacement between the cation and anion centers gives rise to spontaneous polarization.

Since all WZ structures in our research are 5C, this fact can be acknowledged for the discussions below. Besides the c/a ratio for the WZ structure, another important parameter is the critical angle θ when calculating the cation coordination number, which is the minimum angle formed between the fifth anion bond and the existing bonds. According to the statistical data shown in **Figure 1(a)**, an apparently linear relationship has been observed between the critical angle θ and the c/a ratio, indicating that the relative positions of the cations within the trigonal bipyramidal coordination are generally consistent across all materials. Except for nitrides, oxides, and CdS, which favor the WZ structure, most other materials actually exhibit a preference for the ZB structure. Additionally, almost all materials are distributed across the red and blue regions, with materials that have a ZB ground state predominantly located in the blue region (except for CdSe, HgS and HgSe). These materials, when arranged in the WZ structure, tend to show a stretched state (*i.e.*, $c/a > 1.633$), which is less stable than the ZB structure from an energy perspective. In contrast, materials with a WZ ground state are exclusively found in the red region, indicating that only under c -axis compression can the WZ structure maintain a lower energy than the ZB structure. Naturally, this leads to the question as to why WZ materials require a compressed structure to remain energetically favorable.

This issue may be attacked from both the lattice structure and electronic structure

perspectives. As is well-known, the WZ structure consists of two sets of hexagonal lattices (**Figure 1(b)**), and similarly, the cations in these *h.c.p.* structures exhibit distortions, as shown in **Table 2**. Interestingly, all of their c/a axial ratios are greater than the ideal value (1.633). In fact, such distortions are quite common, and some metals exhibit compressed axial ratios. On the one hand, the relationship between the d -electron energy level and the axial ratio is asymmetric,¹⁵ which means it shifts with different rates upon compressing or dilating the lattice along c -axis. On the other hand, there is a correlation between the number of d -electrons and the axial ratio, where c/a tends to increase when the d -electron shell approaches filling. Moreover, strong mixing of s and p orbitals can compress the axial ratio, like in the case of Zn and Cd.¹⁶ Yet, in the case of Be, p – p bonding is found to further reduce the c/a ratio.¹⁶

Table 1. The c/a axial ratio and θ angle of all IIIA-V and IIB-VI compounds arranged in the WZ structure.

IIIA-V	c/a	θ (degree)	IIB-VI	c/a	θ (degree)
BN	1.6539	70.2426	ZnO	1.6150	71.2822
BP	1.6582	70.1412	ZnS	1.6400	70.381
BA_s	1.6548	70.1846	ZnSe	1.6436	70.2558
AlN	1.6034	71.7858	ZnTe	1.6453	70.2135
AlP	1.6416	70.4171	CdO	1.5826	72.5592
AlAs	1.6437	70.3446	CdS	1.6269	70.8242
AlSb	1.6469	70.2412	CdSe	1.6315	70.6757
GaN	1.6293	70.8139	CdTe	1.6404	70.3614
GaP	1.6478	70.2316	HgO	1.5416	75.8854
GaAs	1.6479	70.2438	HgS	1.6321	70.786
GaSb	1.6488	70.2291	HgSe	1.6348	70.6758
InN	1.6163	71.2593	HgTe	1.6421	70.3924
InP	1.6417	70.3811			
InAs	1.6423	70.3815			
InSb	1.6400	70.4237			

Table 2. The c/a axial ratios of several *h.c.p.* IIB and IIIA metals.

Metal	Al	Ga	In	Zn	Cd
c/a	1.654	1.644	1.642	1.827	1.888

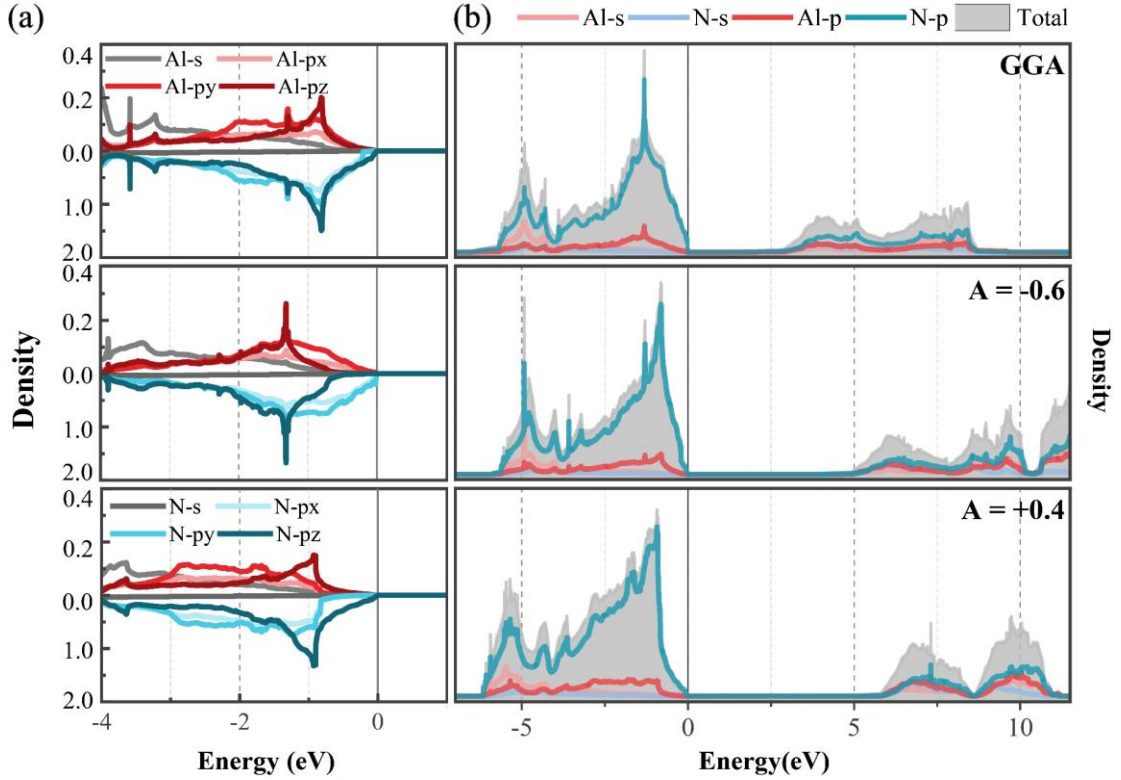


Figure 2. (a) Density of states (DOS) for the *p*-orbital electron components, calculated with shell DFT+A-1/2 at various A values. (b) Partial DOS (PDOS) of AlN, calculated with shell DFT+A-1/2 at various A values.

The phenomena above can be analyzed using the polar plate model shown in **Figures 1(c) and 1(d)**. In metal *h.c.p.* structures, the electrode plates formed by the metal atoms are connected through electronic interactions. The length of the *c*-axis is regulated by the Coulomb interactions between the electrons and the plates, as well as between the plates themselves. Whether an elemental metal adopts a stretched or compressed *h.c.p.* structure depends on quite complicated situations, including the size of the metal atom. For instance, larger atoms Ti/Zr/Hf typically constitute a compressed *h.c.p.* structure, possibly because of the over-large spacing between layers; smaller atoms such as Zn and Cd can show a stretched *h.c.p.* to increase the layer-layer distance. Nevertheless, even this trend is not consistent through an entire row of transition metals. In the WZ structure, an additional layer of anion-based electrode plates is inserted between the metallic layers, and thus, apart from Coulomb interactions, the size and electronegativity of the inserted anions also play a vital role in determining the length

of the c -axis. Bonding between the metal cation and the inserted anion now becomes a central issue in WZ compounds.

The electronic structure approach exactly emphasizes the type of bonding in ferroelectrics. The ferroelectricity of doped hafnia and perovskite ferroelectric materials is related to their indispensable covalent component in bonding.^{4,26} It follows that AlN also has a strong covalent nature in its Al-N bond. **Figure 2** presents the PDOS of AlN calculated through conventional GGA. Near the Fermi level, the Al- p orbitals overlap with the N- p orbitals, exhibiting a consistent shape, which indicates covalency. However, the contribution of N- p electrons is several times higher than that of Al- p electrons, suggesting that the strong electronegativity of N and the metallic nature of Al lead to a significant ionic character in the system. Although it is challenging to experimentally provide a suitable method to explore the impact of ionic or covalent character, first-principles calculations permit us to investigate this issue by altering atomic properties in a hypothetical manner. In particular, the DFT-1/2 method introduces the so-called self-energy potentials in solids,²³ which rectifies the spurious electron self-interaction that usually exists in local density approximation (LDA) or GGA calculations. For covalent compounds, the method is extended to shell DFT-1/2.²² While these methods aim at predicting rectified band gaps, they may also be utilized to perturb the electronegativity of specified atoms,²⁷ where the strong self-energy potential is usually modulated by a factor A ($+A$). Here we employed the shell DFT+A-1/2 algorithm to study the influence of chemical bonding on the geometric structure. It modifies the pseudopotential of the specified atomic shell, tuning the strength of the self-energy potential calculation in that region, which adjusts the electronegativity of the specified atom and further affects its bonding state. When the A value is set between -1 and 0, a reduction in electronegativity occurs; at $A = 0$, the original GGA calculation is retained; and with A values from 0 to 1, the electronegativity of the specified atom is increased. The greater the absolute value of A , the more significant the modification of electronegativity.²⁷ Hence, the objective is to manually set the Al-

N bonds more ionic, or more covalent, in order to explore the consequences.

Following this approach, we have adjusted the electronegativity of the N atom, with inner and outer self-energy potential cut-off radii set to 0.8 and 2.4 bohr, respectively. These values were obtained variationally, since they could maximize the band gap according to the basic principle of DFT-1/2. And **Figure 2(b)** shows the PDOS of AlN calculated using shell DFT+A-1/2, with different A values. When A is set to -0.6, the electronegativity of N is significantly reduced, enhancing the covalency of the system. Compared to conventional GGA calculations, the first peak of the valence band (VB) below the Fermi level shifts deeper, and electrons from the lower VB move toward the VB maximum. The increased electron density at the top of the VB suggests a greater tendency for electrons to participate in covalent bonding, strengthening the system's covalency. At the VB maximum, the primary contributions from Al and N come from the p_x and p_y orbitals, with minimal contribution from p_z (**Figure 2(a)**). This indicates weaker and longer Al-N bonds in the z direction, leading to an elongation of the c -axis (**Figure 4(a)**). When A is set to 0.4, the electronegativity of N increases, significantly reducing the density of states at the VB maximum, and the electron energy levels shift deeper, indicating enhanced electron localization and stronger ionic bonding. At this point, p_z becomes dominant, and Al-N bonding in the z direction strengthens. Compared with *h.c.p.* Al, the insertion of a layer of N allows the Al-N bonds to effectively counteract the elongation, compressing the c -axis and increasing θ . Therefore, systems with stronger ionicity tend to have stronger bonding in the z direction, aiding in c -axis compression, lowering the electronic energy, and enhancing overall system stability. Such conclusion helps to reach a proper interpretation of our GGA results. Although the p_x , p_y , and p_z orbitals at the top of the VB exhibit similar intensities (*cf.* **Figure 2**), p_z shows a slight dominance, allowing AlN to maintain a stable ferroelectric WZ structure.

In **Table 3**, the total DOS contributions for different orbital components within the -1

eV to Fermi level range are recorded for all materials, where the sum of p -orbital components ($p_x+p_y+p_z=1$) and d -orbital components ($d_{xy}+d_{xz}+d_{yz}+d_{z^2}+d_{x^2-y^2}=1$) are normalized to 1. In other Al-V compounds, the proportion of p_z is consistently lower than that of p_x and p_y , indicating that the ionic character is insufficient to support the five-fold coordination. Although the p_z orbital does not appear to dominate in WZ materials aside from aluminides, it is noteworthy that these materials contain d -electrons, which play a significant role in metal close packing. For WZ ground-state materials, the d_{z^2} orbital shows a relative advantage, suggesting that d -electron bonding is directional, with stronger bonding in z direction.

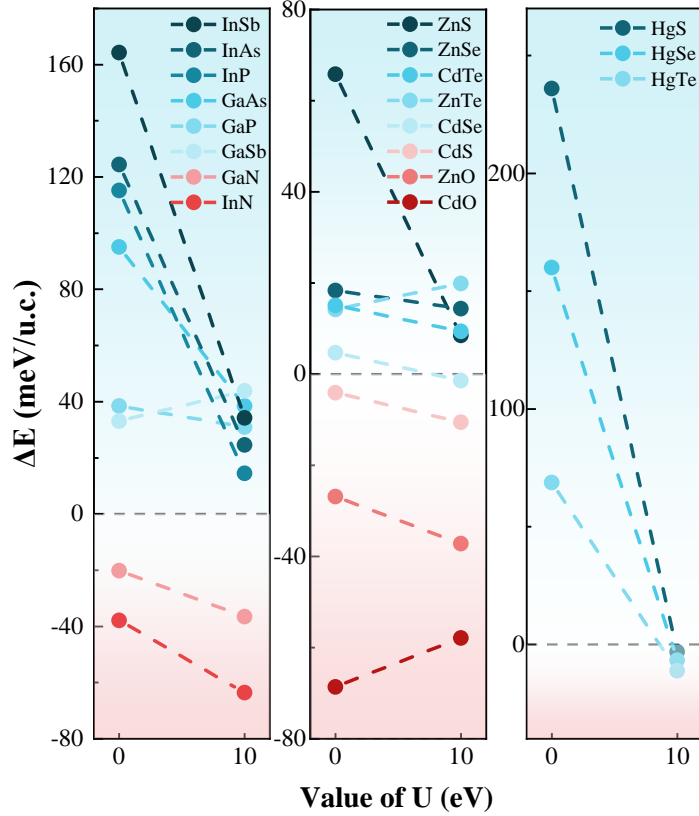


Figure 3. Energy change $\Delta E = E_{WZ} - E_{ZB}$ before and after the DFT+U treatment. On-site Hubbard U correction was performed on the d -electrons of cations only, with $U = 10$ eV and $J = 0$. A smaller ΔE value hints at a more stable WZ structure against the ZB structure.

In the previous section, we selected Al-V systems without d -electrons and discussed the significant influence of p -electrons on the θ parameter. Similar to the impact of d -

electrons on the c/a ratio in metals, d -electrons also affect the θ value in WZ structures. To investigate the influence of d -electrons in metals, we employed the DFT+U method. An on-site Hubbard U correction of 10 eV was applied to the d shells of the metal atoms (**Figure 3**). In all systems (except GaSb, ZnTe, and CdO), ΔE decreased with the consideration of a $U > 0$, rendering the WZ structure more energetically favorable. Notably, for mercury compounds and CdSe, after applying this method, the ground-state structure shifted from ZB to WZ, indicating that d -electrons contribute to the formation of the WZ structure. On the one hand, d -electrons are unfavorable for stabilizing the wurtzite structure. By suppressing the influence of d -electrons through the algorithm, their impact on the system is reduced, allowing the WZ structure to become more favorable. This effect seems to arise from the fact that fully filled d -electrons tend to increase the c/a ratio in metals. On the other hand, as valence electrons, d -electrons participate in bonding. When the DFT+U method is applied, the energy levels of the filled d -shell electrons are effectively lowered, enhancing the metallic character of the cations, reducing their contribution to the VB and weakening the covalent bond strength, which in turn increases the ionic character of the system. This demonstrates that the metallicity of the cations can influence the ground-state geometry.

Table 3. The proportion of the density of states (DOS) contributed by the p and d orbital components within the energy range from -1 eV to the Fermi level.

	p_x	p_y	p_z	d_{xy}	d_{xz}	d_{yz}	d_z^2	$d_{x^2-y^2}$
BN	0.35	0.433	0.217					
BP	0.388	0.456	0.157					
BAs	0.375	0.442	0.183					
AlN	0.221	0.375	0.404					
AIP	0.289	0.444	0.267					
AlAs	0.294	0.443	0.263					
AlSb	0.305	0.437	0.258					
GaN	0.29	0.432	0.278	0.213	0.114	0.162	0.263	0.248
GaP	0.318	0.429	0.253	0.218	0.121	0.161	0.244	0.256
GaAs	0.316	0.427	0.258	0.216	0.121	0.161	0.249	0.253
GaTe	0.322	0.423	0.255	0.214	0.124	0.161	0.247	0.254

InN	0.285	0.423	0.292	0.21	0.116	0.164	0.266	0.244
InP	0.303	0.43	0.267	0.21	0.121	0.167	0.254	0.247
InAs	0.302	0.428	0.27	0.209	0.121	0.168	0.258	0.245
InTe	0.307	0.42	0.273	0.208	0.122	0.165	0.259	0.245
ZnO	0.276	0.422	0.302	0.194	0.111	0.17	0.272	0.254
ZnS	0.239	0.466	0.295	0.146	0.091	0.193	0.274	0.297
ZnSe	0.257	0.476	0.267	0.145	0.089	0.206	0.253	0.306
ZnTe	0.254	0.482	0.264	0.144	0.088	0.208	0.251	0.309
CdO	0.22	0.402	0.378	0.157	0.094	0.156	0.317	0.276
CdS	0.241	0.427	0.332	0.152	0.091	0.188	0.289	0.28
CdSe	0.242	0.425	0.332	0.148	0.089	0.192	0.288	0.283
CdTe	0.247	0.444	0.309	0.146	0.09	0.202	0.274	0.289
HgO	0.323	0.366	0.31	0.244	0.095	0.09	0.318	0.254
HgS	0.306	0.416	0.277	0.211	0.123	0.164	0.262	0.24
HgSe	0.301	0.416	0.283	0.208	0.122	0.167	0.265	0.237
HgTe	0.302	0.423	0.275	0.207	0.123	0.173	0.259	0.238

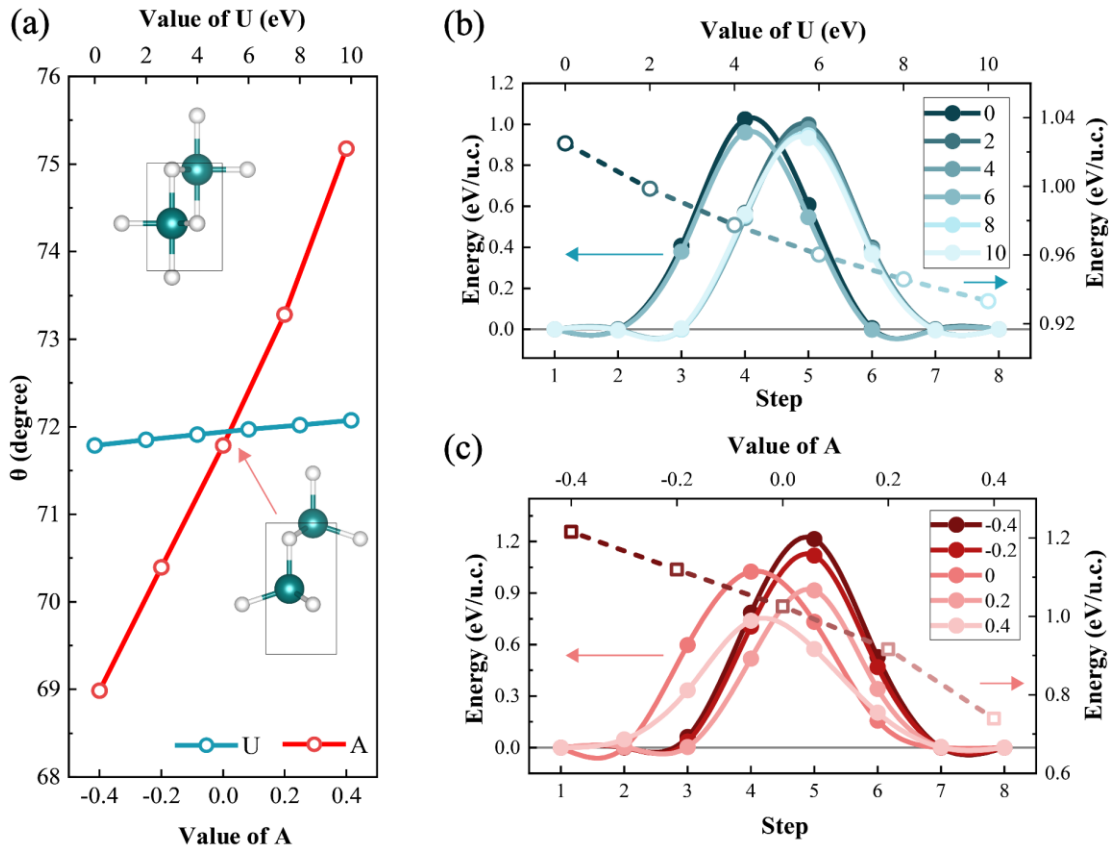


Figure 4. CI-NEB results for WZ AlN: (a) DFT+U calculations applied to Al- p electrons, (b) Shell DFT+A-1/2 calculations applied to N atoms, and (c) changes in the angle θ with varying A and U values.

Figure 4 shows the influence of the Hubbard U correction (DFT+ U) and self-energy potential perturbation (shell DFT+A-1/2) on the bond angle θ in AlN. The effect of a non-zero A value on the structure is more pronounced (**Figure 4(a)**). A higher positive A value, for example, helps to identify the structure of AlN under an abnormally high ionicity that may only be reached artificially. When A is set to 0.6, θ reaches 90° (as shown in the inset structure in **Figure 4(a)**). Further increases in the A value have no additional effect on θ . In this case, the two Al-N bond lengths along the c -axis become equal, and the two N atoms are equivalent. Al is located at the center of a polyhedron coordinated by five N atoms, and this structure does not exhibit spontaneous polarization. Such a phenomenon is not surprising, as this conclusion can be naturally extended from the seven-coordination theory in hafnia-based ferroelectrics.⁴ θ can be understood as a parameter that characterizes the strength of ionicity in the system. The larger the value of θ , the greater the deviation from the critical angle of 65° , indicating that Al can provide more spatial volume for N_5 , stabilizing the 5C configuration. Additionally, the maximum coordination number supported by the $P6_3mc$ structure is 5, meaning that when θ approaches 90° , further increasing ionicity does not alter the coordination number, leading to a maximum value of $\theta_{\max} = 90^\circ$. The distribution of θ in **Figure 1(a)** supports this viewpoint, that materials with stronger ionicity tend to be located in the upper-left region of the diagram, exhibiting more pronounced compressive effects. The most ionic material, HgO (not shown in the figure), has a rock salt ground-state structure. When relaxed in the WZ structure, HgO shows a more favorable WZ configuration with the strongest compressive effect among all materials ($c/a = 1.5416$, $\theta = 75.8854^\circ$). Conversely, materials with stronger covalent character exhibit more pronounced tensile effects, and the materials located at the lower-right end of the diagram, such as borides BP, BAs, and BN, display this tendency.

Moreover, the value of θ directly influences the height of the polarization switching barrier. The intermediate structure of AlN is very similar to the state with $\theta = 90^\circ$. In other words, the larger the θ , the closer the Al atom in the up or down polarization state

is to the center of the hexagonal bipyramid, rendering it closer to the intermediate state of polarization switching. Accordingly, the switching path becomes shorter, a point proven by **Figures 4(a)** and **4(b)**. At the same time, an increase in θ also implies a reduction in spontaneous polarization, as the distance between the centers of the cations and anions shortens. Hence, the parameter θ can be regarded as a significant reference or descriptor in determining the possible emergence of WZ structure and even ferroelectricity.

Conclusion

While the switching dynamics of WZ ferroelectrics are believed to be much simpler than hafnia-based ferroelectrics, there is still a critical question for the origin of the hexagonal WZ structure in compounds like AlN, against the ZB structure. In contrary to the traditional way of coordination number identification, which lists ZB and WZ compounds as 4C compounds, the newly proposed mixed length-angle definition of coordination number identifies the WZ structure as in a 5C state for the cation. The increased coordination number is related to the higher ionicity in WZ compounds compared with ZB compounds. Bonding along the *c*-axis in WZ structures is positively correlated with ionicity; stronger ionic interactions enhance bonding in this direction, reducing the *c/a* ratio and increasing the bond angle θ . A larger θ provides more space for the fifth anion, stabilizing the five-coordinated structure. Additionally, an increased θ brings the polarized structure closer to the intermediate state of polarization switching, thereby lowering the switching barrier. To reduce the coercive field through doping, one can replace cations with elements of higher metallicity or anions with elements of higher electronegativity.

Acknowledgement

This work was supported by the National Key R&D Program of China under Grant No. 2023YFB4402302.

Appendix

The coordination number theory based a mixed consideration of bond length and bond angles is explained in **Figure 5**. Based on the cation in a binary compound, for example, it counts the number of anions surrounding the cation that can be considered as forming bonds with it.

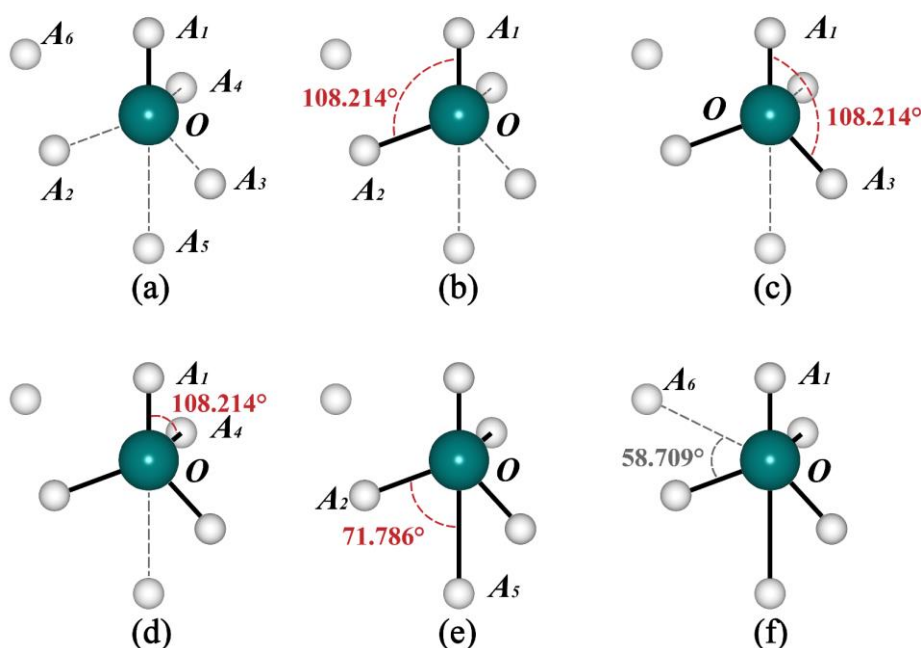


Figure 5. Schematic diagram of coordination number calculation.

- a) The target atom is labeled as O , and the surrounding atoms are labeled A_1 , A_2 , A_3 , etc., in order of increasing distance from the target atom.
- b) The bond angle A_2-O-A_1 is calculated. If this angle is greater than 65° , A_2 is included in the coordination number.
- c) The bond angles between A_3 and the atoms already included in the coordination number, such as A_3-O-A_1 and A_3-O-A_2 , are calculated. The smallest angle is selected, and if it is greater than 65° , A_3 is included in the coordination number.
- d) This process is repeated iteratively until the smallest bond angle involving A_n is less than 65° , at which point the coordination number is determined to be $n-1$.

Figure 5 illustrates a five-coordinated system calculated using this theory, where the minimum bond angles for **A₁** through **A₅** are all greater than 65°, and thus are included in the coordination number. However, **A₆** is excluded, as its minimum bond angle is 58.709°, which is less than 65°.

References

- 1 M. H. Park, Y. H. Lee, T. Mikolajick, U. Schroeder and C. S. Hwang, *MRS Communications*, 2018, **8**, 795–808.
- 2 T. S. Böske, J. Müller, D. Bräuhäus, U. Schröder and U. Böttger, *Appl. Phys. Lett.*, 2011, **99**, 102903.
- 3 S. Fichtner, N. Wolff, F. Lofink, L. Kienle and B. Wagner, *Journal of Applied Physics*, 2019, **125**, 114103.
- 4 J.-H. Yuan, G.-Q. Mao, K.-H. Xue, N. Bai, C. Wang, Y. Cheng, H. Lyu, H. Sun, X. Wang and X. Miao, *Chem. Mater.*, 2023, **35**, 94–103.
- 5 P. Wang, D. Wang, S. Mondal, M. Hu, J. Liu and Z. Mi, *Semicond. Sci. Technol.*, 2023, **38**, 043002.
- 6 K. Ferri, S. Bachu, W. Zhu, M. Imperatore, J. Hayden, N. Alem, N. Giebink, S. Trolrier-McKinstry and J.-P. Maria, *Journal of Applied Physics*, 2021, **130**, 044101.
- 7 J. Huang, Y. Hu and S. Liu, *Phys. Rev. B*, 2022, **106**, 144106.
- 8 D. Wang, P. Wang, B. Wang and Z. Mi, *Applied Physics Letters*, 2021, **119**, 111902.
- 9 A. Bendahah, D. Bensaid, A. Yhaia, M. Khadidja, M. Nouredine, D. Bendouma and Y. Al-Douri, *emergent mater.*, DOI:10.1007/s42247-024-00756-4.
- 10 D. Wang, S. Mondal, J. Liu, M. Hu, P. Wang, S. Yang, D. Wang, Y. Xiao, Y. Wu, T. Ma and Z. Mi, *Applied Physics Letters*, 2023, **123**, 033504.
- 11 W. Zhu, F. He, J. Hayden, J. I. Yang, P. Tipsawat, J.-P. Maria and S. Trolrier-McKinstry, *Applied Physics Letters*, 2023, **122**, 242902.
- 12 S. Calderon, J. Hayden, S. M. Baksa, W. Tzou, S. Trolrier-McKinstry, I. Dabo, J.-P. Maria and E. C. Dickey, *Science*, 2023, **380**, 1034–1038.
- 13 J. Hayden, M. D. Hossain, Y. Xiong, K. Ferri, W. Zhu, M. V. Imperatore, N. Giebink, S. Trolrier-McKinstry, I. Dabo and J.-P. Maria, *Phys. Rev. Materials*, 2021, **5**, 044412.
- 14 Z. Liu, X. Wang, X. Ma, Y. Yang and D. Wu, *Applied Physics Letters*, 2023, **122**, 122901.
- 15 J. X. Zheng-Johansson, O. Eriksson and B. Johansson, *Phys. Rev. B*, 1999, **59**, 6131–6138.
- 16 U. Häussermann and S. I. Simak, *Phys. Rev. B*, 2001, **64**, 245114.
- 17 G. Kresse and J. Furthmüller, *Phys. Rev. B*, 1996, **54**, 11169–11186.
- 18 G. Kresse and J. Furthmüller, *Computational Materials Science*, 1996, **6**, 15–50.
- 19 J. P. Perdew, K. Burke and M. Ernzerhof, *Phys. Rev. Lett.*, 1996, **77**, 3865–3868.
- 20 P. E. Blöchl, *Phys. Rev. B*, 1994, **50**, 17953–17979.
- 21 G. Kresse and D. Joubert, *Phys. Rev. B*, 1999, **59**, 1758–1775.
- 22 K.-H. Xue, J.-H. Yuan, L. R. C. Fonseca and X.-S. Miao, *Computational Materials Science*, 2018, **153**, 493–505.
- 23 L. G. Ferreira, M. Marques and L. K. Teles, *Phys. Rev. B*, 2008, **78**, 125116.
- 24 G.-Q. Mao, Z.-Y. Yan, K.-H. Xue, Z. Ai, S. Yang, H. Cui, J.-H. Yuan, T.-L. Ren and X. Miao, *J. Phys.: Condens. Matter*, 2022, **34**, 403001.
- 25 G.-Q. Mao, H. Yu, K.-H. Xue, J. Huang, Z. Zhou and X. Miao, *J. Mater. Chem. C*, 2024, **12**, 15463–15474.
- 26 R. E. Cohen, *Nature*, 1992, **358**, 136–138.

27J. Huang, W. Yang, Z. Chen, S. Yang, K. Xue and X. Miao, *Physica Status Solidi–Rapid Research Letters*, 2024, **18**, 2300489.